IEEE Access
Multidisciplinary | Rapid Review | Open Access Journal

Received October 15, 2021, accepted November 8, 2021, date of publication November 10, 2021,
date of current version November 19, 2021.

Digital Object Identifier 10.1109/ACCESS.2021.3127242

Rough North Correction Estimation Algorithm Based on Terrain Visibility

ONDREJ NEMEC[1], JAN PIDANIC[1], (Senior Member, IEEE), AND PAVEL SEDIVY[2], (Senior Member, IEEE)

[1]Department of Electrical Engineering, Faculty of Electrical Engineering and Informatics, University of Pardubice, 532 10 Pardubice, Czech Republic
[2]RETIA, a.s., 530 02 Pardubice, Czech Republic

Corresponding author: Jan Pidanic (jan.pidanic@upce.cz)

This work was supported by the European Regional Development Fund (ERDF)/European Social Fund (ESF) "Cooperation in Applied Research Between the University of Pardubice and Companies in the Field of Positioning, Detection and Simulation Technology for Transport Systems (PosiTrans)" under Grant CZ.02.1.01/0.0/0.0/17_049/0008394.

ABSTRACT The article describes an innovative algorithm of a radar north correction estimation. The uniqueness of the algorithm is the pure data/software nature without need for any additional north-seeking equipment. This procedure is a key step of a registration local coordinate system to a global one. The presented method is an application of cognitive radar approach, matching of radar ground clutter echoes with a-priori information, vector map data, and terrain elevation profile. The algorithm is based on matching observed ground clutter areas within received radar signal, with (corresponding) areas visible upon terrain profile data. The designed north correction algorithm was tested on real radar signal recorded on the 2D surveillance short-range radar ReVISOR made by RETIA, a.s. The current implementation utilizes SRTM height profile data.

INDEX TERMS Algorithm, coordinates, estimation, ground clutter, north-correction, north-finding, radar, system registration.

I. INTRODUCTION

A radar system is usually used to perform surveillance or tracking of surface, airborne or space targets. Targets are detected and localized in a radar local coordinate system. The local coordinate system of a monostatic primary radar is spherical (for 2D radar systems collapsed to polar projection). The radar local coordinate system is biased and rotated relative to global coordinate systems. Unknown bias of position and orientation denies multi-sensor data fusion and effective use of data (e.g. interpretation over map). Real world applications require a radar local coordinates system registration to a global coordinates system, and consequent conversion of measured target coordinates to the global system. The typical global coordinate systems used for non-space targets are geodetic systems, e.g. WGS-84, UTM or S-JTSK [1].

Coordinate system conversions are well documented non-linear transformations. Registration of the coordinate system includes translation of a radar local coordinate system to radar position in the global coordinates system, and rotation of the local coordinates system altitude, to achieve mutual alignment with the global coordinates system. Position of radar can be easily measured by GNSS (like GPS, Galileo, GLONASS, Beidou) or determined by a geodetic method [2]. Measurement of local coordinate system altitude alignment relative to the global one is more challenging.

Mutual attitude of these coordinate systems can be expressed by the set of three angles: Roll, Pitch and Yaw. Ground based radar systems are usually operated in the leveled position. Leveling is done using the gravitation force vector. Pitch and roll angles are, as a result, negligible values. The angular correction of the radar local coordinates system reduces, in this case, to the yaw angle bias estimation. The negative value of the yaw angle is also called the north correction as it describes the difference between the radar (instrumental) azimuth and the real geographic north pole. This correction aligns the local instrumental zero azimuth with the geographic north pole.

North correction can be estimated using magnetic compass measurement of the direction bias relative to the Earth's magnetic pole. Second group of methods uses a gyrocompass based on gyroscopic effects of the Earth rotation or

The associate editor coordinating the review of this manuscript and approving it for publication was Hongwei Du.

relativistic aspects of this rotation. Another alternative is a GNSS compass which uses two GNSS antennas/receivers and searches for a heading, which aligns the difference of measured pseudoranges to projections of the antennas' base [3]. The projection is calculated using a known satellite elevation angle [4]. In general, devices used to estimate north correction are called north-seekers (NS). NS devices are usually independent units mounted on the general radar system.

A magnetic compass requires a complex time variable model of magnetic declination [5], and in addition cannot be usually used to estimate north correction when mounted on a radar system. The performance is limited by use of ferromagnetic materials in construction and impact of power electronics. Ferromagnetic material remanent field and power electronic current generated field influence the geomagnetic field near a radar system [6].

Gyrocompasses are based on spinning mass, fiber optic gyroscope (FOG), or ring laser gyroscope (RLG) [7]. Spinning mass-based gyrocompasses use gyroscopic and precession effects to automatically align with the south-north direction [2]. FOG and RLG gyrocompasses use Sagnac's effect and cannot perform automatic alignment with south-north direction. Therefore, FOG and RLG are used as sensing elements for north correction calculus [7]– [9]. All these devices need very precise production and calibration processes making these devices accurate at the expense of a relatively high price for many applications [2].

GNSS NS devices use principles of moving baseline RTK (Real-Time-Kinematic) positioning based on comparison of the carrier phase between two spatially displaced GNSS antennas with known mutual position. GNSS NS are very sensitive to signal propagation conditions and especially to multipath effect. The price of these devices is moderate [10].

North correction can be also estimated by a group of methods using a monocular or a camera mounted collinearly with a radar antenna electrical boresight. One of the methods is based on mutual direction measurements between a military artillery compass and radar antenna (with mounted monocular). True azimuth to a radar device is measured by the military artillery compass after its aiming at the radar antenna. Azimuth correction can be evaluated using a bearing sensor readout when the antenna, according to the mounted monocular, aims toward the artillery compass. An alternative to this method is aiming the antenna monocular or camera towards an object with known position, and consequently calculating the inverse geodetic problem. All these procedures are done by a radar system operator or semi-automatically by SW (software) with the aid of a system operator. The accuracy of these methods depends on the equipment used, range of object, and operator skills. The main disadvantage of those methods is dependence on weather conditions and other problems related to production – sights must be adjusted on antenna test range. Sight or camera is hard to replace by a spare in the field without compromising accuracy.

North correction estimation, as with any other measurement process, is subject to errors. Any north correction error necessarily leads to a determined target coordinates error which occurs after target coordinates conversion to the global coordinate system. Errors of north correction are either caused by the NS device and/or by NS mounting to the radar device [2], [11].

The NS device produced errors can be divided into systematic or random errors. A NS device is usually equipped with a set of mitigation algorithms to compensate its inner generated systematic errors (e.g. temperature drifts) [2]. Random errors can be averaged out at the expense of time.

Target coordinates are measured in the coordinate system of an antenna and measurement is converted, using an antenna bearing sensor, to the local radar coordinate system. A NS device must be accurately placed on the radar system to precisely determine orientation with respect to the antenna, otherwise NS origin bias error occurs. To minimize measurement error the NS device should be exactly mounted on a precisely machined surface and the origin bias error of NS sub-system and antenna must be calibrated. Calibration is done during the radar system production, repair, or maintenance (maintenance with intervention to NS-antenna system critical parts e. g. replacement of NS device or antenna). The calibration is usually not compatible with rapid repairs in the field. Calibration can be avoided at the cost of extreme precision of mechanical construction and machining (mounting accuracy).

The article describes a software-based north correction estimation method based on alignment of surveillance radar (with rotating antenna) ground clutter echoes with visible parts of terrain. The visible parts of terrain are estimated from a digital elevation model (DEM) of the area surrounding the radar.

The DEM is usually arranged into tiles, where each tile covers the spatial area. The resolution (size of each tile) varies on different DEM formats such as GTOPO30 [12], ASTER [13], SRTM [14], [15] or any other DEMs provided by national mapping agencies. The SRTM (Shuttle radar topology mission) DEM data were used for algorithm principal verification and demonstration.

Radar data can be gathered by any monostatic primary ground-based radar. In our case, we use radar data collected by REVISOR, a X-band short range radar produced by RETIA, a.s. [16].

The algorithm's principle comes from feature matching navigational methods [2]. The key difference is that position of radar is known, and feature matching is used just for north correction estimation. The key advantage of the proposed algorithm is that current hardware can be used to estimate north correction. North correction is also estimated directly in the radar local coordinate system and no further calibration is needed during radar production (in comparison with other methods).

The original idea was to develop a north correction algorithm based on point reflectors outlined in [17], and marked as ''fine''. The fine algorithm proved to have reasonable precision but may be very complex to evaluate and may produce

ambiguous results (this ''fine'' algorithm will be presented in detail in a separate paper). We have found a less complex and less precise, but much easier to perform, alternative algorithm marked as ''rough''. The rough algorithm is described in this article. A combination of fine and rough algorithms (rough algorithm use as initial estimate) leads to efficient, precise, and unambiguous results.

The algorithms require sufficient and stable terrain roughness properly described by the DEM model and may fail on sites like tundra, desert, steppe, or savanna.

The presented algorithm can be modified for modern Active Electronic Steering Array (AESA) radar systems with sector scanning and discrete sampling of space.

The article is organized in four main chapters. In the first chapter we describe the developed algorithm principle and input data in detail. The second chapter focuses on effects and the algorithm's constrains influencing north correction accuracy. Chapter number four presents the algorithm's achieved results for various radar sites with different operating conditions.

II. THE ROUGH NORTH-SEEKER CORRECTION ALGORITHM PRINCIPLE

A received radar signal consists of target echoes, various types of clutter, and noise. The dominant part of clutter is ground clutter, which is spatially stationary. The radar ground clutter signal originates from visible terrain surface reflection and ground-based objects. Surface based reflections dominate at the most of radar sites. Ground clutter signal can be extracted out of the received radar signal using Doppler processing and averaging. This clutter signal can be fit to a theoretical clutter visibility model.

The radar ground clutter radio visibility (model) is similar to optical visibility. The radio visibility can be evaluated by the various Line of Sight (LoS) methods [18] using a DEM model. The magnitude of the ground clutter RCS within the radar resolution cell cannot be directly obtained from the macroscopic terrain model (relative to radar wavelength) and behaves as a random variable influenced by the number of the ground-based reflectors, their materials, and geometry of the reflecting surfaces. The ground clutter reflectivity cannot be reasonably predicted from the DEM data. The only obtainable information is ground clutter presence.

The ground clutter DEM visibility model and received signal-based ground clutter model are angularly biased (one degree of freedom, yaw/north coordinate). The bias estimate can be used for north correction. The yaw bias north correction estimator is based on mutual correlation of the clutter visibility model with the ground clutter signal. The ground clutter visibility model is represented by a binary matrix. The clutter signal is converted to a binary matrix by thresholding. The proposed algorithm is outlined by block diagram in Fig. 1. and details of algorithm are described in following paragraphs.

Ground clutter based on the received signal model and ground clutter visibility model (DEM based) are

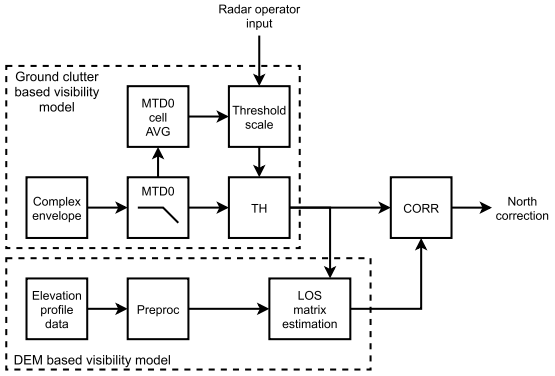

FIGURE 1. Block diagram of the algorithm (MTD0 - Moving Target Detector zero channel filter, TH - thresholding, AVG - averaging, CORR - correlation function computation, Preproc - Elevation profile data pre-processing).

implemented in individual branches and described in subsections A a B respectively. The outputs from both branches are processed by cyclic correlation and finally used for north-correction estimation.

A. SIGNAL BASED CLUTTER MODEL

The ground clutter presence within individual resolution cells is evaluated using amplitude of MTD0 (Moving Target Detector - zero channel) [19] filtered received signal. The filtered signal contains ground clutter echoes, slow moving target echoes, and noise. The slow-moving target echoes could be, if significant, averaged out combining signals of multiple turns. The noise signal is suppressed in subsequent processing (thresholding). The ground clutter signal dominates the output signal. In addition, signal averaging suppresses ground clutter fluctuation.

$$B_R(m,n) = \begin{cases} 1; & \text{if } |S(R_m.\phi_n)| > T_H \\ 0; & \text{otherwise.} \end{cases} \quad (1)$$

where B_R is a radar binary image/matrix, $S(R_m, \phi_n)$ is a complex envelope, R_m is a radial range of the m-th resolution cell, ϕ_n is an azimuth of the n-th resolution cell, T_H is a threshold level.

The visibility of ground clutter for individual resolution cells is evaluated by thresholding. The threshold level is determined from the MTD0 noise cell amplitude average. According to the experience, the threshold T_H should be about 20 dB above this average. The algorithm was verified with this threshold scale for many sites under various conditions. Results of individual resolution cells amplitude comparison, with threshold T_H, form a ground clutter visibility binary matrix B_R (1) illustrated in Fig. 2.

B. DEM BASED CLUTTER MODEL

The algorithm in the second branch evaluates terrain surface visibility using DEM. The evaluation is performed for areas equivalent to individual resolution cells. DEM data sets typically include elevations for individual latitude and longitude coordinates. Data sets are chunked into individual ''tiles''

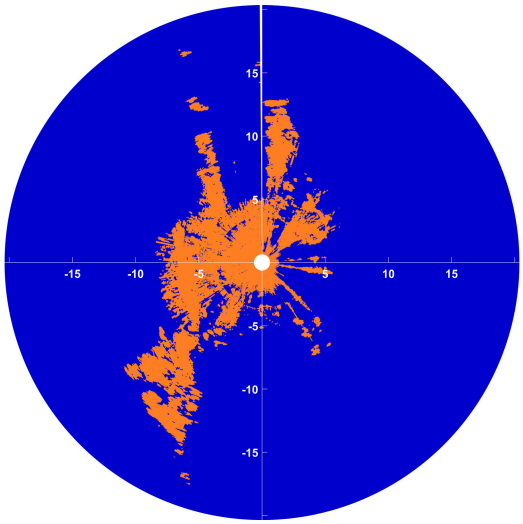

FIGURE 2. Ground clutter visibility binary matrix B_R polar plot.

with resolution of 1 or 3 arc seconds (roughly corresponding to 30 m or 90 m). LOS evaluation of terrain visibility requires a DEM matrix including all radar resolution cells up to the instrumental range. The DEM elevation data use is illustrated on the SRTM data set, freely available from [14]. SRTM data can be replaced by any other relevant DEM data. The algorithm was tested using the 1 arc second SRTM data. The terrain visibility evaluation algorithm interpolates the DEM matrix over a line from the radar origin to the center of individual radar resolution cells. The result of interpolation allows evaluation of visibility (shadowing).

The terrain visibility evaluation algorithms process the elevation profile matrix E (2). This matrix includes elevation above mean sea level for every single resolution cell of the DEM model used. The algorithm further utilizes two vector of coordinates, latitude (3) and longitude (4), which correspond to matrix rows and columns respectively. Both vectors describe an axis with constant step.

$$E = \begin{pmatrix} T(X_i, Y_n) & \cdots & T(X_j, Y_n) \\ \vdots & \vdots & \vdots \\ T(X_i, Y_m) & \cdots & T(X_j, Y_m) \end{pmatrix} \quad (2)$$

$$X_E = \left[X_i, X_i + \Delta X, X_i + 2 \cdot \Delta X, \ldots, X_j + 1^\circ\right] \quad (3)$$

$$X_E = \left[Y_m, Y_m + \Delta Y, Y_m + 2 \cdot \Delta Y, \ldots, Y_n + 1^\circ\right] \quad (4)$$

where E is the elevation profile matrix, T is the DEM tile, $X_{i,j}$ and $Y_{m,n}$ are latitude and longitude coordinates of individual tiles, X_E is the latitude coordinate vector of matrix E, Y_E is the longitude coordinate vector of matrix E.

Elevation profile point coordinates are converted to new a polar coordinate system using inverse geodetic problem (IGP) calculus (5) [20]. DEM data is converted from the latitude-longitude coordinate system into a local tangential plane polar coordinate system by linear interpolation (6). Use of the linear interpolation method does not reduce overall

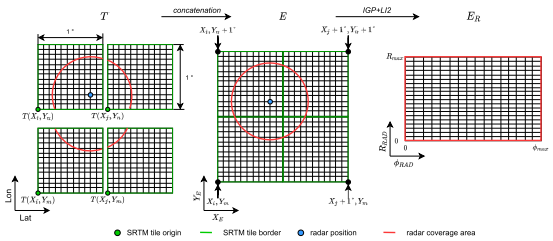

FIGURE 3. Example of DEM preprocessing for SRTM 1 arc second data.

algorithm performance. The process is depicted in Fig. 3.

$$[R_E, \phi_E] = \mathrm{IGP}\left(X_{RAD}, Y_{RAD}, X_E, Y_E\right) \quad (5)$$

$$E_R = \mathrm{LI2}\left(E, R_E, \phi_E, R_{RAD}, \phi_{RAD}\right) \quad (6)$$

where R_E is the slant range vector of matrix E, ϕ_E is the azimuthal angle vector of matrix E, IGP is the inverse geodetic problem, X_{RAD} and Y_{RAD} are latitude and longitude coordinates of the radar, E_R is the elevation profile matrix interpolated into polar coordinates, LI2 is the general linear interpolation function.

LoS visibility is individually evaluated for every single point (Resolution Cell Under Test, RCUT) in the polar coordinate system.

LoS is evaluated by comparison of all DEM data points between RCUT and the phase center of the radar antenna above mean sea level with points of connection line $E_C\left(R_k, R_i, \phi_j, h_{APC}\right)$ (7). Any terrain elevation above the connection line results in no visibility and is represented by a zero value in $B_L\left(R_i, \phi_j, h_{APC}\right)$. In the opposite case RCUT visibility B_L value is set to one. Individual evaluation results $B_L\left(R_i, \phi_j, h_{APC}\right)$ (8) form a binary visibility matrix B_L. The process is illustrated in Fig. 4.

$$E_C\left(R_K, R_i, \phi_j, h_{APC}\right) = \frac{E_R\left(R_i, \phi_j\right) - E_R\left(0, \phi_j\right) - h_{APC}}{R_i} \cdot R_k + \left(E_R\left(0, \phi_j\right) + h_{APC}\right) \quad (7)$$

$$B_L(R_i, \phi_j, h_{APC}) = \begin{cases} 1; & \text{if all} \\ & E_C\left(R_k, \phi_j\right) > \\ & E_R\left(R_k, R_i, \phi_j, h_{APC}\right), \\ & \text{for } R_k \in (0, R_i) \\ 0; & \text{otherwise.} \end{cases} \quad (8)$$

where E_C is the elevation of the connection line between radar and resolution cell with coordinates R_i and ϕ_j, computed for the resolution cell R_k and ϕ_j, and antenna phase center height h_{APC}. B_L is binary visibility matrix.

The terrain visibility evaluation algorithm reference implementation is based on geometrical optics (infinitely narrow antenna beam). This procedure provides reasonable accuracy for radar systems with narrow antenna beam in azimuth (validated for radar system with instrumented range of 18 km and antenna beamwidth of 2 degrees). For system with wider antenna beam the result can be improved by blurring the

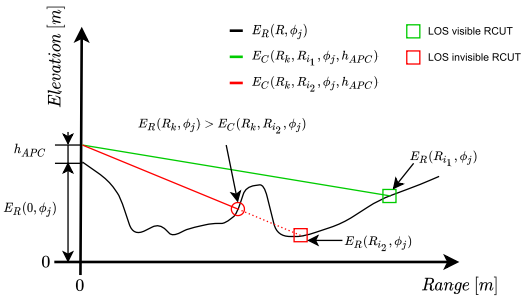

FIGURE 4. LOS evaluation illustration.

theoretical terrain visibility matrix by the antenna radiation pattern.

The results of the LOS matrix evaluation were verified by comparison with Cambridge Pixel Radar Coverage Tool [21] output. Fig. 5 presents an example of the LOS matrix evaluation algorithm result. Fig. 6 shows Cambridge Pixel Radar Coverage Tool output for the same radar position (zero altitude coverage evaluated). Results of both procedures match each other. The minor differences are caused by the different DEM model used. Our implementation utilizes 1 arc second resolution SRTM data (approx. resolution of 30 meters) [14], while the Cambridge Pixel uses 3 arc seconds DEM model resolution (approx. resolution of 90 meters) [15], [21].

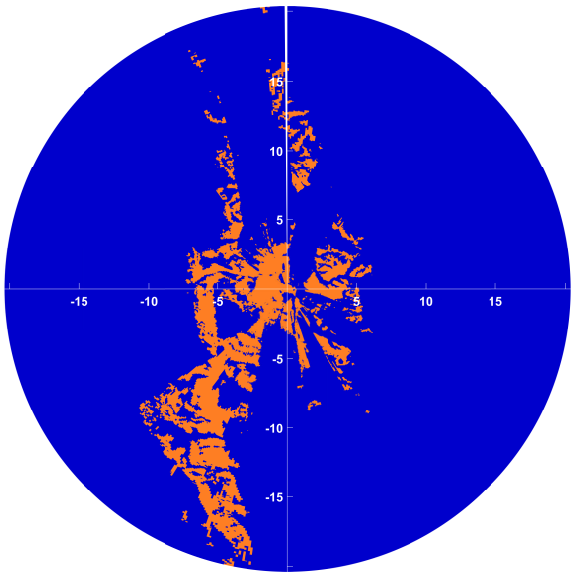

FIGURE 5. Computed elevation profile data for radar height above terrain 2 m by described algorithm.

The evaluated LOS matrix is based on the DEM model and like any other model-based method provides limited validity and may produce local inaccuracies. Local terrain elevation variations, e. g. slopes, ripples, and ditches, within a single DEM resolution cell are averaged out and represented by a single value. Deviation of real terrain elevations from the DEM model may be even a few meters for typical DEM resolution. Exactness of the LOS evaluation would be optimal

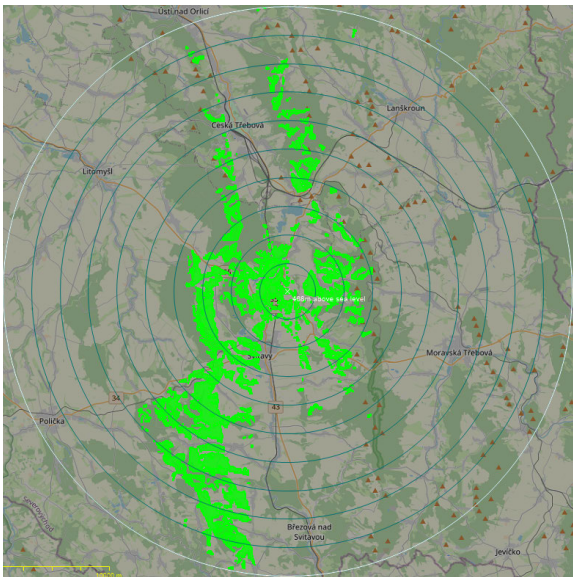

FIGURE 6. Computed elevation profile data for radar height above terrain 2 m by Cambridge Pixel – Radar Coverage Tool.

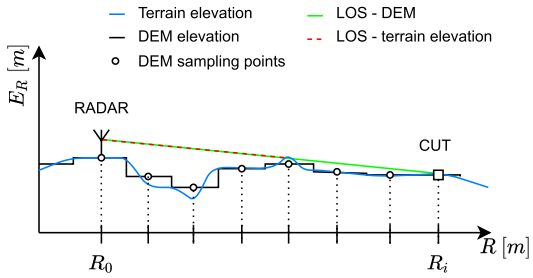

FIGURE 7. DEM caused LOS error demonstration.

if DEM data contained maximum elevation of terrain instead of average elevation value. This would improve shadowing effect estimation. The inaccuracy of the LOS matrix evaluation is caused by use of average elevation instead. This effect is illustrated in Fig. 7.

The algorithm is quite sensitive to the origin of visibility for evaluation exactness. This origin is represented by the antenna phase center position (latitude, longitude, and height above sea level). Accuracy of these input variables (based on position measurement, e.g. GNSS) is typically in order of meters. The most severe influence on visibility evaluation is related to height inaccuracy. Small changes of antenna phase center height have a huge impact on the visibility behaviour. This effect is equivalent to landscape visibility when climbing to the view tower. Even small changes of height may cause significant difference of visibility, and height measurement error may move the visibility estimation origin just around this threshold.

The algorithms must include an additional procedure to mitigate the height inaccuracy impact. The mitigation technique is based on speculative change of antenna height (represented by antenna phase center height) and evaluation of visibility for every position of origin. If the visibility

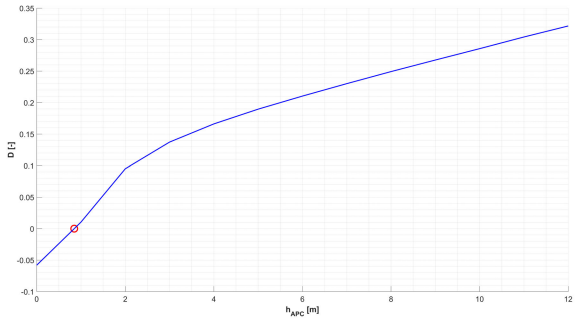

FIGURE 8. Demonstration of h_{APC} influence on difference of non-zero elements of binary visibility matrix for h_{APC} and radar binary matrix.

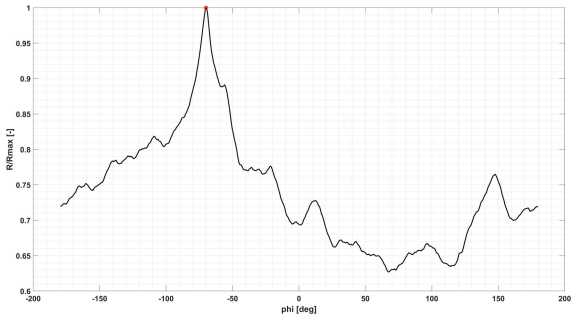

FIGURE 9. Normalized correlation function with marked maximum by red circle for binary images Fig. 2 and Fig. 5.

estimation origin is too low, the model validity is violated by excessive shadowing. Conversely, when the origin is too high, model validity is disrupted by an excessive number of cells with visible terrain. We have found an empirical method to select the antenna phase center height within the validity region. This method is based on comparison of a number of visible clutter cells. Radar ground clutter visibility is compared to the DEM visibility model and selects the antenna h_{APC} with the closest number of cells in both models.

Visibility evaluation for heights deviated up to 3 meters from the nominal antenna phase center height is typically sufficient to find a valid model parameter. This parameter range must be additionally limited to heights above ground level. The number of visible cells grows with rising h_{APC} (left region in Fig. 8). The number of visible DEM model cells typically meets the number of visible radar ground clutter visibility cells (zero value of (9), outcome of (10)), red circle in Fig. 8). Further rise of the h_{APC} parameter results in a rapid rise of visible DEM model cell numbers (background cells dominants, mid region in Fig. 8). An additional rise of h_{APC} causes a slower rise of the DEM model visible cells (background cell visibility "saturation" right region in Fig. 8).

$$D\left(h_{APC}\right) = \sum_{\phi_R}\sum_{R_R} B_L\left(h_{APC}\right) - \sum_{\phi_R}\sum_{R_R} B_R \tag{9}$$

$$h_{apcopt} = \operatorname{argmin}\left[\left|D\left(h_{APC}\right)\right|\right] \tag{10}$$

where $D\left(h_{APC}\right)$ is the difference of non-zero elements of the binary visibility matrix computed for h_{APC}, and the radar binary matrix h_{apcopt} is the optimal antenna phase center height in terms of shadowing.

The final step of the rough correction algorithm is evaluation of the radar ground clutter visibility model azimuth bias. Azimuth bias estimation is based on correlation (cyclic in azimuth, average all range quanta) according to (11). The north correction estimation conforms to bias with the maximum of the correlation function (Fig. 9).

$$R_L\left(\phi_L\right) = \sum_{R_R}\sum_{\phi_R} B_R\left(R_R, \phi_R\right) \cdot B_{ML}\left(R_R, \phi_R - \phi_L\right) \tag{11}$$

where R_L is cyclic correlation function of radar binary matrix and maximum likelihood binary visibility matrix B_{ML} computed for h_{apcopt}. Alternative approach of the north correction evaluation is the use of modified binary matrices B_R and B_L containing -1 instead of 0. This modification should be more sensitive to absenting visibility area shape, nevertheless the output north correction differences are negligible.

III. EFFECTS INFLUENCING ACCURACY

This discussion is focused on method strengths and limitations identified during processing on real radar signal records with reference implementation of the algorithm.

There are two groups of effects influencing accuracy. The first group is related to DEM model exactness and the second group originates from radar observation. The DEM model effects include elevation profile inaccuracy, artificial ground objects, measurement subject of errors, and DEM model ageing. Radar observation effects are related to non-ground clutter reflections.

Elevation profile inaccuracy is the most severe effect. The terrain visibility is affected by local variances of terrain elevation within the DEM resolution cell represented by a single elevation value. The typical origin of these variances is terrain slope, and railway/road embankments. This effect is significant even for a quite small DEM resolution cell size.

Another important effect rises from artificial ground objects (e.g., buildings, towers, poles, and vegetation). These objects may cause shadowing of terrain surfaces and reflect impacting signal (cause ground clutter presence). Presence of this ground clutter is unpredictable from DEM. Shadowing effects may especially hide substantially large areas and cause significant difference of real and computed LOS binary matrices. This effect is illustrated in Fig. 10,11 and Fig. 12, and Fig. 13, where radar data includes ground clutter free sectors shadowed by artificial ground objects. These areas are marked by red lines. This effect might be partially mitigated using vector map data (e.g. OpenStreetMap [22]). Use of map data leads to a significant increase of complexity.

The DEM model is typically a result of measurement, and as with any other measurement, is subject to errors. These errors may originate not only from random impacts, but incorporate additional non-random effects (e.g. buildings reflectivity observed by SAR radar at the time of acquisition of The Shuttle Radar Topography Mission - SRTM).

The last identified effect is DEM model ageing. The typical example of this effect is a newly built road or railway.

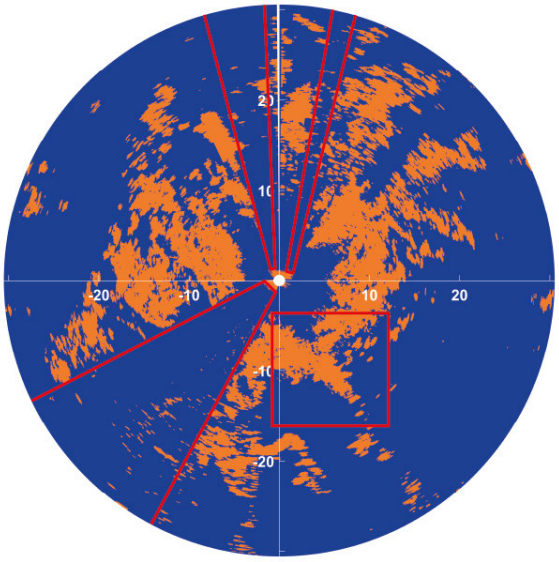

FIGURE 10. The radar data with model inaccuracies (site Rajhrad): Radar binary matrix.

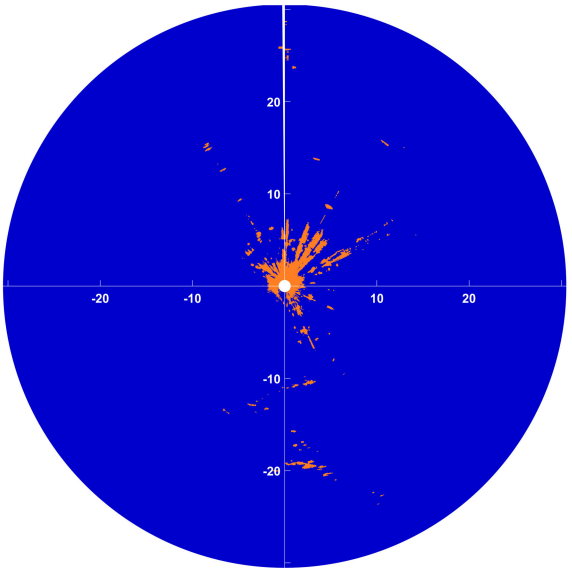

FIGURE 12. The radar data with model inaccuracies (site Stare Jesencany): Radar binary matrix.

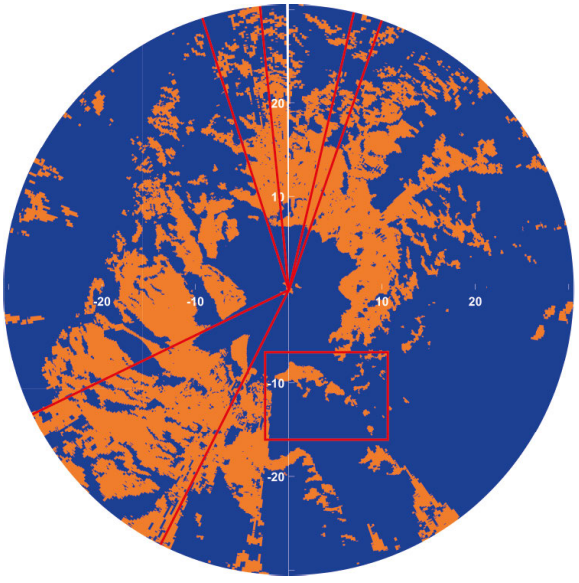

FIGURE 11. The radar data with model inaccuracies (site Rajhrad): LOS matrix.

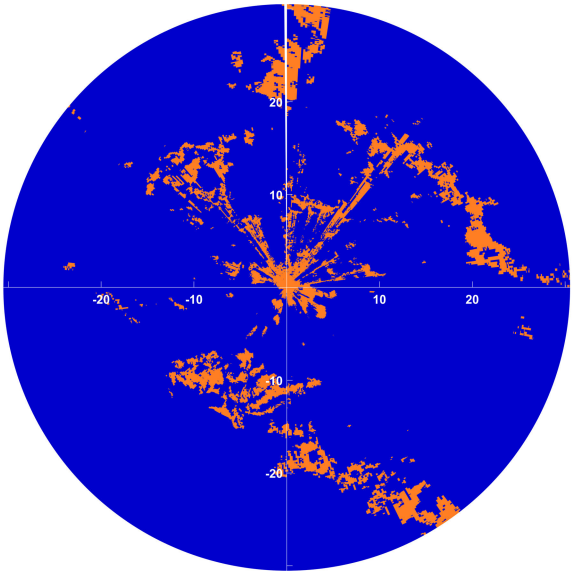

FIGURE 13. The radar data with model inaccuracies (site Stare Jesencany): LOS matrix.

The radar observation effect most often influencing north correction estimation is weather clutter. Areas containing rain or snow clouds with zero radial velocity are indistinguishable from ground clutter and unpredictable from the DEM model. The effect is shown in Fig. 14, 15. Weather clutter is often weaker than ground clutter and impact on north correction estimation accuracy could be mitigated by the preference of the strongest reflections (increase of threshold).

IV. ALGORITHM RESULTS

North seeking algorithm was implemented in MATLAB^{TM} [23] combining existing libraries (e.g. SRTM and radar processing). The algorithm can be implemented in any programming language supporting double precision of float point numbers.

Algorithm was verified on real signals recorded on 2D X band ReVISOR surveillance short-range radar developed by RETIA, a.s. [16]. Processed signals are complex envelope samples for individual range quanta and pulse repetition intervals (PRIs). The signal is augmented for each PRI with relevant meta data (antenna position relative to azimuth instrumental origin). Individual signal records were complemented by radar antenna position. Radar position was measured using GPS (L1 only receiver, code measurement).

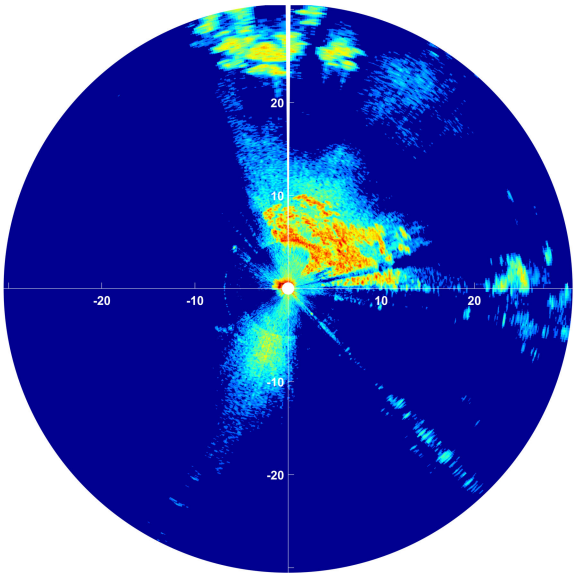

FIGURE 14. The radar data with rain (site Zalesi): amplitude data (blue the weakest, orange the strongest signal).

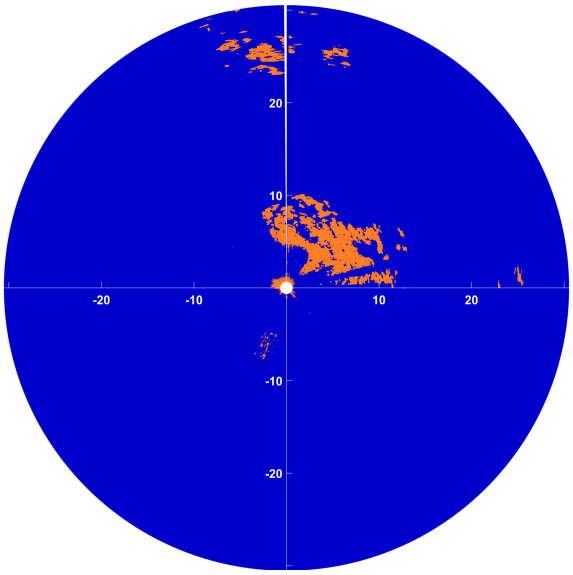

FIGURE 15. The radar data with rain (site Zalesi): LOS matrix.

Antenna phase height initial value was based on GPS measurement. Terrain surfaces LOS matrix evaluation suffered from this GPS height measurement inaccuracy. The only remedy we found is above-described phase height (h_{APC}) variation procedure. Use of SRTM data for h_{APC} instead of GPS measurement, considered as an alternative, gained no benefit.

The signals were recorded at various sites, seasons, and environment conditions within a mid-European region (countryside environment). All sites included within instrumental range of sensor undulating landscape areas. Records from complete flat sites were not available.

For every radar signal record was available north correction gained from optical aiming to object with known coordinates

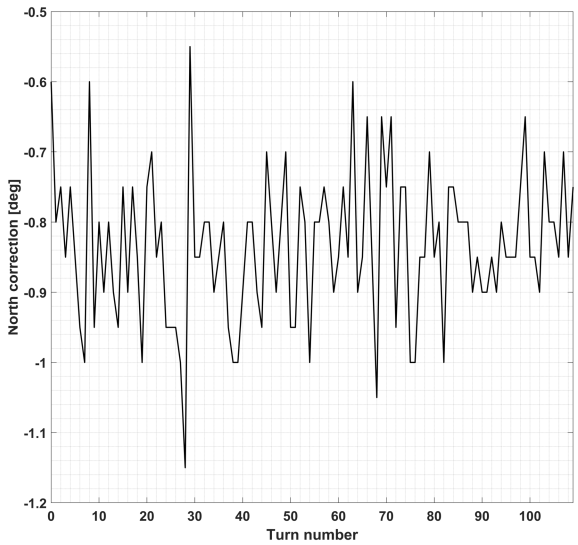

FIGURE 16. Delta error of north correction computed for 110 radar turns and radar site Svitavy.

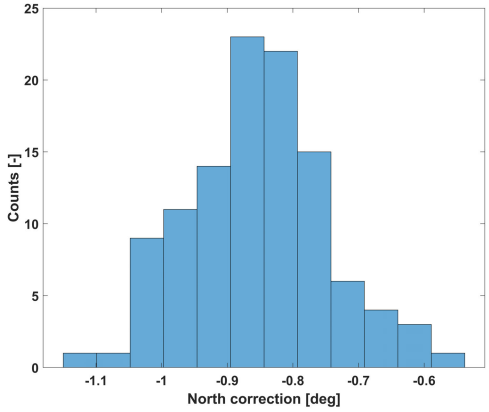

FIGURE 17. Histogram of delta error of north correction computed for 110 radar turns and radar site Svitavy.

(e.g. communication tower) and inverse geodetical problem calculus. This north correction values were as a reference for algorithm precision evaluation.

North correction estimation algorithms processed for every radar signal record multiple turns. Time series of this north correction estimates was analyzed and result of this analyzes is presented in Table 1. Estimates for individual turns are generally biased, and this bias from true north correction is included in table aside random component statistics. No correlation of error random components among individual estimates was observed (e.g. Fig. 16). Estimate histogram of 110 north correction estimates for individual turns is presented in Fig. 17.

The presented rough algorithm provides reasonable accuracy for fine north correction algorithm based on matching point ground clutter echoes (method overview in [17]). The initial estimate reduces computation complexity of the fine algorithm calculus and mitigates potentially ambiguity of individual ground clutter reflector mutual association.

TABLE 1. The radar data with rain (site Zalesi): LOS matrix.

Site name	Coor--dinates LAT LON	Ref. North correc--tion [deg]	Avg. north correc--tion [deg]	Avg. error [deg]	Max. error [deg]	Error RMS [deg]
Svitavy	49.796 16.495	-0.85	-0.8345	0.0155	0.30	0.1068
Rajhrad	49.036 16.644	0.25	-0.26	-0.50	0.75	0.56
Stare Jesencany	50.002 15.746	0.00	-0.08	-0.10	1.00	0.29
Zalesi	50.415 15.778	0.70	-0.59	-1.28	1.70	1.29

V. CONCLUSION

The paper presents the novel north seeking software-based data aided algorithm utilizing elevation profile data (SRTM) and received ground clutter echoes. The algorithm is intended for radar sites with direct visibility of undulated terrain and was validated using real radar signal data records (recorded in multiple sites within the Central Europe region). Perform analysis identify significant impact of antenna phase center inaccuracy and algorithms was augmented by heuristic method to mitigate this effect.

The algorithm achieves reasonable accuracy, unambiguity, and reliability. The presented method is intended as an initial estimate for a more precise method utilizing point ground clutter reflectors. The algorithm reliability can be improved by using 3D models buildings and vegetation based on vector map data (e.g. Open street map).

REFERENCES

[1] L. Zhiping, Q. Yunying, and Q. Shubo, *Geodesy—Introduction to Geodetic Datum and Geodetic Systems*, 1st ed. Berlin, Germany: Springer, 2014.
[2] P. Groves, "Principles of GNSS, inertial, and multisensor integrated navigation systems," in *Proc. 10th Optical Fiber Sensors Conf.*, Glasgow, Scotland, 2014, p. 442.
[3] *VN-300 Quick Start Guide*. Accessed: Oct. 1, 2021. [Online]. Available: https://www.vectornav.com/resources/quick-start-guides/vn-300-quick-start-guide
[4] M. L. Sollie, T. H. Bryne, and T. A. Johansen, "Pose estimation of UAVs based on INS aided by two independent low-cost GNSS receivers," in *Proc. Int. Conf. Unmanned Aircr. Syst. (ICUAS)*, Atlanta, GA, USA, Jun. 2019, pp. 1425–1435.
[5] *Magnetic Declination (Variation) | NCEI*. Accessed: Feb. 8, 2021. [Online]. Available: https://www.ngdc.noaa.gov/geomag/declination.shtml
[6] R. B. Langley, "The magnetic compass and GPS," Innovation, GPS World, Univ. New Brunswick, New Brunswick, NJ, USA, Tech. Rep., Sep. 2003.
[7] R. B. Dyott and D. E. Allen, "Fiber optic gyroscope north finder," in *Proc. 10th Int. Conf. Opt. Fibre Sensors*, Glasgow, Scotland, Sep. 1994, p. 442.
[8] G. E. Sandoval-Romero and V. Argueta-Díaz, "A simple theoretical comparison between two basic schemes in function of the earth's north pole detection: The static method," *J. Sensors*, vol. 2010, pp. 1–6, Jan. 2010.
[9] I. S. Kim, Y. Kim, I. A. Matisov, V. A. Nikolaev, V. E. Strigalev, S. Lee, and J. Bae, "Dynamic scheme north finder using a fiber optic gyroscope," *Proc. SPIE*, vol. 2895, pp. 228–236, Nov. 1996.
[10] *Inertial Navigation Primer*. VectorNav Library. Accessed: Feb. 8, 2021. [Online]. Available: https://www.vectornav.com/resources/inertial-navigation-primer
[11] J. Zhang, J. Li, Y. Huang, C. Hu, K. Feng, and X. Wei, "Analysis and compensation of installation errors for rotating semi-strapdown inertial navigation system," *IEEE Access*, vol. 7, pp. 101019–101030, 2019.
[12] *USGS EROS Archive, Digital Elevation, Global 30 Arc-Second Elevation (GTOPO30)*. Accessed: Oct. 3, 2021. [Online]. Available: https://www.usgs.gov/centers/eros/science/usgs-eros-archive-digital-elevation-global-30-arc-second-elevation-gtopo30?qt-science_center_objects=0#qt-science_center_objects
[13] *ASTER Global Digital Elevation Model V003*. Accessed: Oct. 3, 2021. [Online]. Available: https://lpdaac.usgs.gov/products/astgtmv003/
[14] *Earth Resources Observation and Science (EROS) Center—Shuttle Radar Topography Mission (SRTM) 1 Arc-Second Global*. Accessed: Oct. 3, 2021. [Online]. Available: https://www.usgs.gov/centers/eros/science/usgs-eros-archive-digital-elevation-shuttle-radar-topography-mission-srtm-1-arc?qt-science_center_objects=0#qt-science_center_objects
[15] *NASA Shuttle Radar Topography Mission Global 3 Arc Second*. Sioux Falls, SD, USA: NASA JPL, NASA EOSDIS Land Processes DAAC. 2013, doi: 10.5067/MEASURES/SRTM/SRTMGL3.003.
[16] *ReVISOR*. RETIA. Accessed: Feb. 8, 2021. [Online]. Available: https://www.military-retia.eu/en/revisor
[17] O. Nemec, J. Pidanic, and P. Sedivy, "Novel radar north correction estimation algorithm," in *Proc. IEEE Radar Conf. (RadarConf20)*, Florence, Italy, Sep. 2020, pp. 1–6.
[18] L. Floriani and P. Magillo, "Algorithms for visibility computation on terrains: A survey," *Environ. Planning B, Planning Des.*, vol. 30, no. 5, pp. 709–728, Oct. 2003, doi: 10.1068/b12979.
[19] D. C. Schleher, *MTI and Pulsed Doppler Radar With MATLAB*, 2nd ed. Boston, MA, USA: Artech House, 2010.
[20] B. R. Bowring, "The geodesic inverse problem," *Bull. Géodésique*, vol. 57, nos. 1–4, pp. 109–120, Mar. 1983.
[21] *Radar Coverage Tool | Cambridge Pixel*. Accessed: Oct. 1, 2021. [Online]. Available: https://www.cambridge pixel.com/products/tools-accessories/radar-coverage-tool/
[22] *OpenStreetMap*. Accessed: Oct. 1, 2021. [Online]. Available: https://www.openstreetmap.org/
[23] *MathWorks*. Accessed: Oct. 1, 2021. [Online]. Available: https://www.mathworks.com/

ONDREJ NEMEC received the M.Sc. degree from the University of Pardubice, in 2019, where he is currently pursuing the Ph.D. degree. Since 2019, he has been working as a Systems Engineer with RETIA. His professional interests include systems engineering, and radar signal and data processing.

JAN PIDANIC (Senior Member, IEEE) was born in 1979. He received the M.Sc. and Ph.D. degrees from the University of Pardubice, in 2005 and 2012, respectively. His research interests (more than ten years) include signal processing in passive radar systems, bistatic radars, clutter modeling, and optimization of signal processing algorithms with parallel processing techniques.

PAVEL SEDIVY (Senior Member, IEEE) received the M.Sc. degree from Czech Technical University in Prague, in 1999. He is currently pursuing the Ph.D. degree with the University of Pardubice. He also works as the Principal Systems Engineer and the Head of the Technical Support Department with RETIA, a.s. His research interests include systems engineering, radar system design, and the radar signal processing.